Direct determination of monolayer MoS_2 and WSe_2 exciton binding energies on insulating and metallic substrates

To cite this article: Soohyung Park *et al* 2018 *2D Mater.* **5** 025003

2D Materials

OPEN ACCESS

RECEIVED
7 October 2017

REVISED
17 December 2017

ACCEPTED FOR PUBLICATION
3 January 2018

PUBLISHED
11 January 2018

PAPER

Direct determination of monolayer MoS_2 and WSe_2 exciton binding energies on insulating and metallic substrates

Soohyung Park[1,2], Niklas Mutz[3], Thorsten Schultz[1], Sylke Blumstengel[3], Ali Han[4], Areej Aljarb[4], Lain-Jong Li[4,5], Emil J W List-Kratochvil[3], Patrick Amsalem[1] and Norbert Koch[1,2]

[1] Institut für Physik and IRIS Adlershof, Humboldt-Universität zu Berlin, Brook-Taylor Straße 6, 12489 Berlin, Germany
[2] Helmholtz-Zentrum für Materialien und Energie GmbH, Bereich Solarenergieforschung, Albert-Einstein-Straße 15, 12489 Berlin, Germany
[3] Institut für Physik, Institut für Chemie and IRIS Adlershof, Humboldt-Universität zu Berlin, Brook-Taylor Straße 6, 12489 Berlin, Germany
[4] Physical Sciences and Engineering, King Abdullah University of Science and Technology, Thuwal 23955-6900, Saudi Arabia
[5] Corporate Research and Chief Technology Office, Taiwan Semiconductor Manufacturing Company (TSMC), Hsinchu 30075, Taiwan

E-mail: nkoch@physik.hu-berlin.de

Keywords: MoS_2, WSe_2, monolayer transition metal dichalcogenide, electronic structure, excitons, exciton binding energy, UPS, IPES

Supplementary material for this article is available online

Abstract

Understanding the excitonic nature of excited states in two-dimensional (2D) transition-metal dichalcogenides (TMDCs) is of key importance to make use of their optical and charge transport properties in optoelectronic applications. We contribute to this by the direct experimental determination of the exciton binding energy ($E_{b,exc}$) of monolayer MoS_2 and WSe_2 on two fundamentally different substrates, i.e. the insulator sapphire and the metal gold. By combining angle-resolved direct and inverse photoelectron spectroscopy we measure the electronic band gap (E_g), and by reflectance measurements the optical excitonic band gap (E_{exc}). The difference of these two energies is $E_{b,exc}$. The values of E_g and $E_{b,exc}$ are 2.11 eV and 240 meV for MoS_2 on sapphire, and 1.89 eV and 240 meV for WSe_2 on sapphire. On Au $E_{b,exc}$ is decreased to 90 meV and 140 meV for MoS_2 and WSe_2, respectively. The significant $E_{b,exc}$ reduction is primarily due to a reduction of E_g resulting from enhanced screening by the metal, while E_{exc} is barely decreased for the metal support. Energy level diagrams determined at the K-point of the 2D TMDCs Brillouin zone show that MoS_2 has more p-type character on Au as compared to sapphire, while WSe_2 appears close to intrinsic on both. These results demonstrate that the impact of the dielectric environment of 2D TMDCs is more pronounced for individual charge carriers than for a correlated electron–hole pair, i.e. the exciton. A proper dielectric surrounding design for such 2D semiconductors can therefore be used to facilitate superior optoelectronic device function.

Two-dimensional transition-metal dichalcogenides (2D TMDCs) are attractive candidates for next-generation optoelectronic devices due to their unique electronic and optical properties that originate from their low dimensionality and high-symmetry structure [1, 2]. When going from the bulk to a monolayer, 2D TMDCs like MoS_2, $MoSe_2$, WS_2, and WSe_2 exhibit a transition from an indirect to a direct energy gap semiconductor at the K-point of the Brillouin zone (BZ), rendering the electronic properties at this point of reciprocal space particularly relevant for electronic and optical processes. However, some studies reported that the WSe_2 monolayer might actually be an indirect band gap semiconductor with its conduction band minimum (CBM) located at the *Q*-point (see figure 1), albeit this state is almost degenerate with that at the K-point [3, 4]. In addition, in these 2D TMDCs, Coulomb interactions between charges play a prominent role because of spatial confinement and moderate electrostatic screening [5–7]. This leads to the emergence of strongly bound excited state quasiparticles, i.e. excitons [5, 8–12], trions [13–15], and biexcitons [16], which can also be observed at room temperature. The excitonic nature of these excited states is therefore very important for the function of TMDCs based devices, such as light emitting diodes, field effect transistors, optical sensors and photovoltaic cells [17–21].

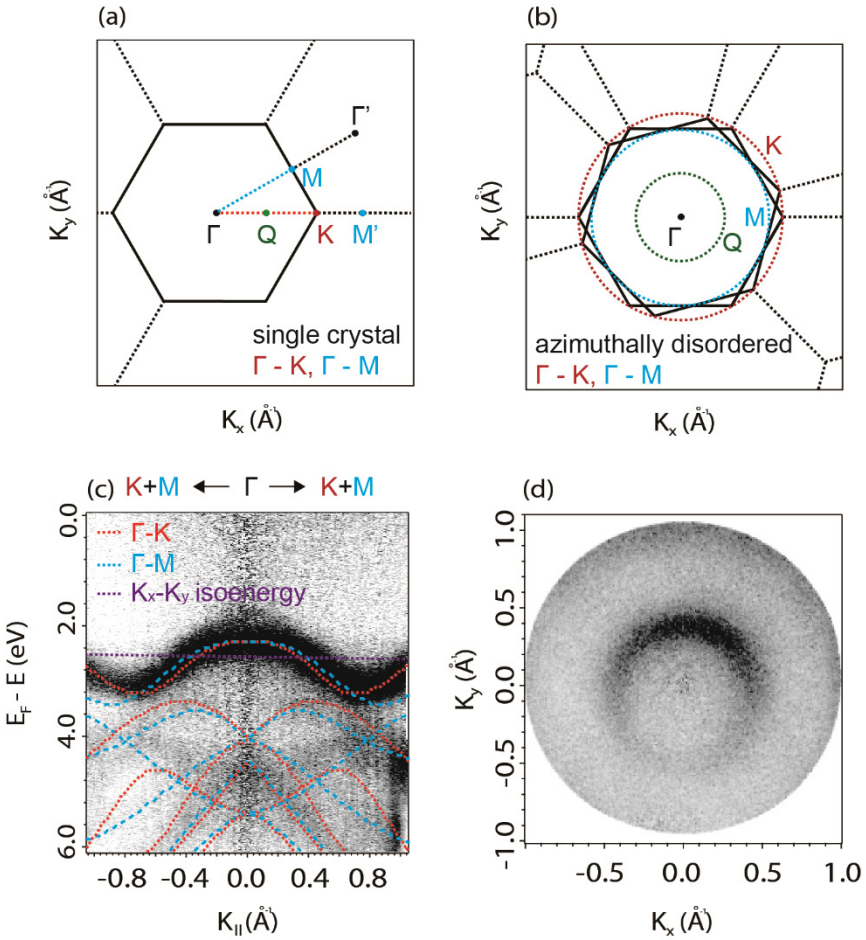

Figure 1. (a) BZ scheme of a single crystalline 2H-TMDC showing the high symmetry points (Red = *K*, Blue = *M* and Green = *Q* point). (b) BZ scheme of an azimuthally disordered 2H-TMDC. The high symmetry points form concentric circles centered around Γ. (c) ARPES (from angle-resolved time-of-flight spectroscopy) spectrum of an azimuthally disordered MoS_2 monolayer on sapphire together with density functional theory calculation results along Γ–*M* (blue dashed lines) and Γ–*K* (red dashed lines). (d) K_x–K_y isoenergy (2.5 eV, violet dashed line in figure (c)) surface from the ARPES spectrum revealing the circular structure due to the azimuthal disorder.

To employ 2D TMDCs in optoelectronic devices, understanding the fundamental physical properties of these quasiparticles is necessary. In this regard, one key parameter is the exciton binding energy ($E_{b,exc}$) [22]. It is the energy difference between the lowest-energy optical absorption, i.e. that of the fundamental exciton (E_{exc}), and the electronic energy gap (E_g). While in many bulk semiconductors with high dielectric constant $E_{b,exc}$ values are exceedingly small and barely noticeable at room temperature [23–26], the reduced screening in 2D TMDCs leads to sizable differences of the fundamental optical gap, i.e. the energy of a correlated electron–hole pair, and the electronic gap, i.e. the energy difference of individual electrons and holes at the band edges [3, 27]. There are reports on the determination of E_g in 2D TMDCs by scanning tunneling microscopy (STM) and photoluminescence (PL) spectroscopy [28–30]. With STM, a conductive substrate is required and only the minimum energy gap (i.e. either direct or indirect) can be measured in a straightforward manner, and several assumptions are needed to estimate E_g from PL measurements as discussed below. Here, we present a direct experimental determination of $E_{b,exc}$ for 2D TMDCs supported on insulator and metal substrates, by comparing E_{exc} with E_g measured at different *k*-points using angle resolved direct and inverse photoelectron spectroscopy, which has not yet been reported.

There are reports on $E_{b,exc}$ values of 2D TMDCs, but they rely on assumptions or approximations, so that higher reliability of these values is still needed. For instance, a hydrogenic Rydberg model has been used to interpret optical measurements and to evaluate $E_{b,exc}$ in 2D TMDCs. In that model, $E^{(n)}_{b,exc}$ is determined using the following equation [13, 31–33]:

$$E^{(n)}_{b,exc} = \frac{\mu e^4}{2\hbar^2 \varepsilon^2_{eff} (n - \frac{1}{2})^2} = E_g - E^{(n)}_{exc} \qquad (1)$$

where $\mu = 1/(m_e^{-1} + m_h^{-1})$ is the effective reduced mass of the hole and electron, ε_{eff} is effective dielectric constant, E_g is the electronic energy gap, and $E^{(n)}_{exc}$ is the *n*th transition energy of the exciton. Here, a ε_{eff} has to be assumed by fitting to the higher order transitions, and cannot be directly measured. In addition, μ, often taken from theoretical calculations, is not a materials

constant as it can be affected by environment-dependent polarization and other parameters, such as contact-induced charge transfer and lattice strain [28, 34–38]. Despite the technological relevance, such attempts to estimate $E_{b,exc}$ have not been done for TMDCs supported by metal substrates, where charge transfer could additionally modify the effective dielectric constant [39]. Another attempt to determine E_g comprised measuring potassium intercalated bulk MoS_2 as a model of a quasi-monolayer [40, 41]. While in this approach valence and conduction (due to filling by electrons from potassium) bands can be observed by direct photoemission, the intercalation could induce strong local electric fields (Stark effect) [42], in addition to the band gap renormalization [39, 43] caused by occupation of the conduction band states [44].

Consequently, here we pursue a direct determination of $E_{b,exc}$ that explicitly includes the influence of the dielectric environment by comparing E_g and E_{exc}. E_{exc} is readily measured by absorption spectroscopy. E_g is obtained from direct and inverse photoelectron spectroscopy, which gives the energy required to create a (photo-) electron and a (photo-) hole, respectively, including the individual electron and hole screening effect. Both methods are applied in an angle-resolved manner to ensure assessing the actual minima and maxima in the band structure. We chose MoS_2 and WSe_2 monolayers, as they are representative 2D TMDCs having n-type and ambipolar character, and they have already been widely studied. To investigate the impact of the supporting substrate dielectric properties, we choose sapphire and Au. Sapphire is a good insulator with a finite dielectric constant ($\varepsilon_r \sim 11.5$) and Au is a conductor with an infinite static dielectric constant. This contributes important application relevant aspects to our results, as the former can be used as gate dielectric in a field-effect transistor, and the latter as electrode material in numerous device types. We determine $E_{b,exc}$ for both TMDCs to be 240 meV on sapphire, and it is more than 100 meV smaller when Au is used as substrate, and we derive the complete energy level alignment of MoS_2 and WSe_2 monolayers on sapphire and Au, respectively.

Since our MoS_2 and WSe_2 monolayer samples on both substrates comprise azimuthally disordered grains, we first explain that the unique band structure of the TMDCs still allows retrieving reliable band structure data with angle-resolved photoelectron spectroscopy (ARPES). Figure 1(a) displays the hexagonal BZ of a single crystalline 2H-TMDC together with the corresponding high-symmetry points. For comparison, the BZ scheme of an azimuthally disordered TMDC layer is shown in figure 1(b), demonstrating that the high-symmetry points form concentric circles centered around Γ. This scheme shows that all azimuthal directions going through Γ are equivalent and go simultaneously through *Q*, *M* and *K*. Commonly, azimuthally disordered (or in-plane polycrystalline) samples do not provide any dispersive features in photoemission spectra due to direction-averaging. However, provided that the individual grains are sufficiently large to exhibit individually the proper band structure, the specificity of the band structure of TMDCs and other layered materials (such as graphite) makes the average dispersion in the radial direction strongly dominated by sharp 1D dispersive states due to Van Hove singularities along the high symmetry Γ–*M* and Γ–*Q*–*K* directions. It was shown that this particular feature enables ARPES studies even with azimuthally disordered samples [45]. Therefore, all the ARPES and angle-resolved inverse photoelectron spectra (ARIPES) spectra presented below mainly include dispersive features in the Γ–*M* and Γ–*Q*–*K* directions. This is clearly visible in figure 1(c), where the ARPES spectrum of an azimuthally disordered (see figure 1(d)) MoS_2 monolayer on sapphire exhibits sharp dispersive features corresponding to the band structure as calculated along the high-symmetry directions (Γ–*M* and Γ–*Q*–*K*). In addition, the linewidth of these features is comparable to previous ARPES reports, which demonstrate the high homogeneity of the studied sample in terms of surface potential [46, 47].

Having established that the main dispersive features can be observed for our samples, we first turn to monolayer MoS_2 supported by sapphire, the respective ARPES and ARIPES spectra are shown in figures 2(a) and (b). For all ARPES spectra displayed in this work, the He I_β satellite was removed to enable reliable onset determination, and the spectra are shown normalized to the first peak for better visibility of energy shift trends. Similarly, ARIPES spectra were deconvoluted to obtain accurate onset values, as detailed in the Experiment Section of the supporting information (SI). As noted above, the ARPES and ARIPES allow us following the band dispersion along the Γ–*M* and Γ–*K* directions simultaneously. By sampling the dispersion beyond the first BZ, the positions of Γ (at 0 $Å^{-1}$), *M* (1.10 ± 0.08 $Å^{-1}$), and *K* (1.24 ± 0.08 $Å^{-1}$) were determined, and they agree with previous results [36]. From the ARPES and ARIPES spectra at Γ, the respective valence band maximum (VBM_Γ) and conduction band minimum (CBM_Γ) are found at 1.78 eV binding energy (BE) and −0.50 eV BE, respectively, resulting in an electronic gap at the Γ-point ($E_{g,\Gamma}$) of 2.28 eV ($E_g = |VBM| + |CBM|$). When increasing the sampled electron momentum parallel to the surface ($k_\parallel$) up to 0.65 $Å^{-1}$, the ARPES spectra exhibit a gradual spectral shift of the VBM towards higher BE. For higher $k_\parallel$ values, VBM shifts back to lower BE until the K-point is reached. The CBM observed in the ARIPES spectra shifts monotonically toward the Fermi level when going from Γ to *M* and *K*. The trend in the spectral evolution, indicated by the arrows in figures 2(a) and (b), reveals a band dispersion matching well with previously reported experimental (ARPES only) and theoretical (both cases) results [3, 36, 38, 48]. The top spectra in

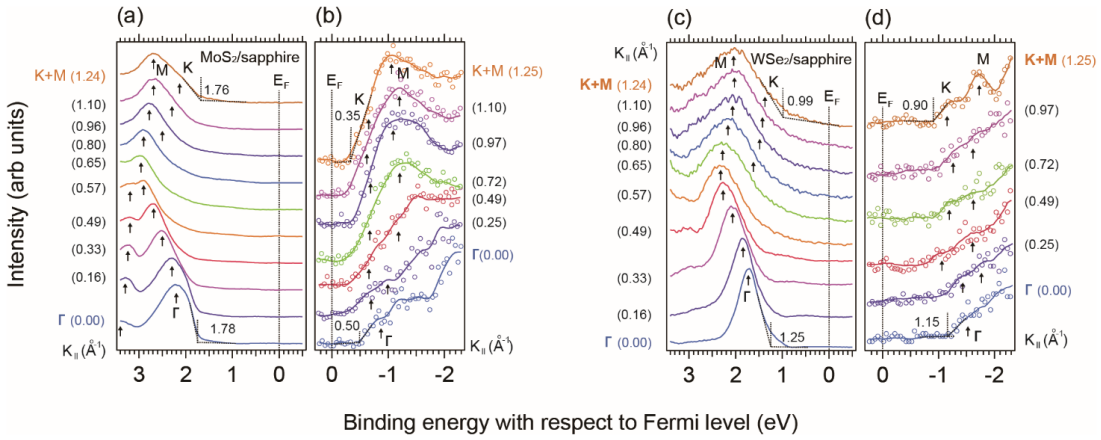

Figure 2. (a) ARPES and (b) ARIPES spectra of MoS_2 on sapphire. (c) ARPES and (d) ARIPES spectra of WSe_2 on sapphire. Both spectra are measured with varying polar angle. The arrows are guides for the band dispersion.

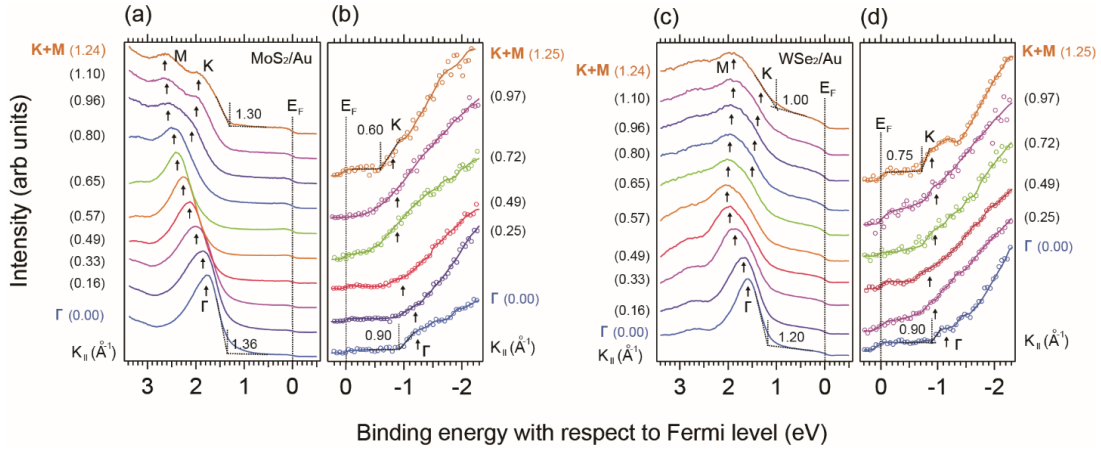

Figure 3. (a) ARPES and (b) ARIPES spectra of MoS_2 on Au. (c) ARPES and (d) ARIPES spectra of WSe_2 on Au. Both spectra are measured with varying polar angle. The arrows are guides for the band dispersion.

figures 2(a) and (b) show the band energies at the K-point (1.24 $Å^{-1}$), from which VBM_K, CBM_K, and the electronic gap at the K-point ($E_{g,K}$) of MoS_2/sapphire were determined to be 1.76 eV BE, −0.35 eV BE, and 2.11 eV, respectively. Notably, this is experimental evidence that a direct band gap occurs at the K-point.

The WSe_2/sapphire band dispersion along the Γ–*M* and Γ–*K* directions, again given as a function of $k_{\|}$, is displayed in figures 2(c) and (d). The bottom spectra at Γ reveal the VBM_Γ and CBM_Γ at 1.25 eV BE and −1.15 eV BE, respectively. Accordingly, $E_{g,\Gamma}$ for WSe_2/sapphire is determined to be 2.40 eV. Due to the same structure (twofold hexagonal symmetry), the evolution of the WSe_2/sapphire bands as a function of $k_{\|}$ in the ARPES and ARIPES spectra is similar to that of MoS_2/sapphire in figures 2(a) and (b). Nonetheless, important differences are observed: (i) MoS_2 appeared as strong n-type semiconductor [49, 50] while WSe_2/sapphire displays more ambipolar character [51] and (ii) as a result of strong valence spin–orbit splitting, the full width at half-maximum of the WSe_2/sapphire valence band features at the K-point is broader than that of MoS_2/sapphire, in agreement with previous results [3]. The VBM_K, CBM_K, and $E_{g,K}$ key values for WSe_2/sapphire were determined to be 0.99 eV BE, −0.90 eV BE, and 1.89 eV, respectively.

To quantify the influence of a metallic medium, such as a metal contact, on $E_{b,exc}$, we investigated MoS_2 and WSe_2 monolayers on polycrystalline Au substrates. In analogy to the results shown for the TMDCs on sapphire above, figures 3(a) and (b) show the ARPES and ARIPES spectra of MoS_2/Au along the Γ–*M* and Γ–*K* directions, simultaneously. From the bottom spectra, VBM_Γ and CBM_Γ are determined to be 1.36 eV BE and −0.90 eV BE, respectively, resulting in an $E_{g,\Gamma}$ of 2.26 eV. Similarly, at the K-point, VBM_K and CBM_K, were determined to be 1.30 eV BE and −0.60 eV BE, respectively, resulting in $E_{g,K}$ of 1.90 eV. Note that MoS_2 appears more p-type on Au as compared to sapphire. This could be due to the coupling to the metal and the different effective work function of Au compared to sapphire, as a strong chemical interaction can be ruled out from the absence of chemically shifted core levels (see figure S3 in SI). Given that the Fermi level is found far from both conduction and valence band edges eventual charge transfer due to Fermi level pin-

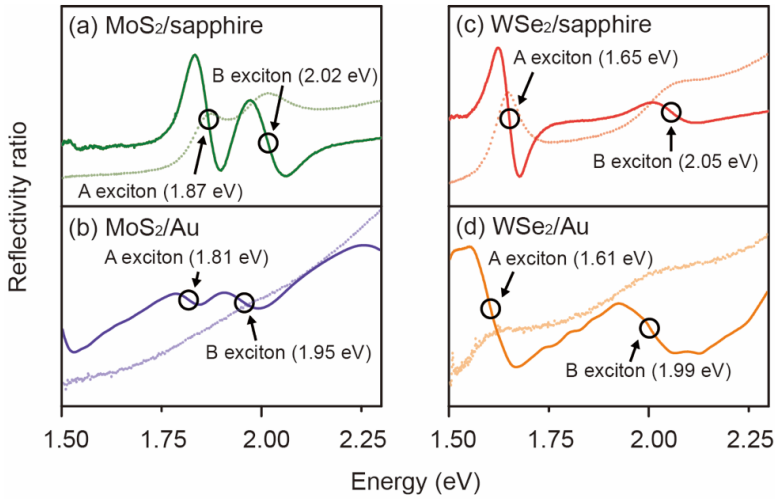

Figure 4. Measured reflectance spectra (dashed lines) and the first derivative of the reflectance spectra (solid lines) $[\frac{d}{dE}(\log(R_0/R))]$ of (a) MoS_2 on sapphire, (b) MoS_2 on Au, (c) WSe_2 on sapphire and (d) WSe_2 on Au. The circles denote the energy position of the A and B exciton.

ning should be minimal. Importantly, we observe that $E_{g,K}$ for MoS_2/Au is decreased by 0.21 eV compared to MoS_2/sapphire. Most of this difference is expected to originate from a more efficient screening of the electron/hole final states by the metal electrons. In addition, as is discussed further below, a change in charge carrier density due to charge transfer between MoS_2 and Au can result in band gap renormalization [28, 35, 52] and in differently screened ARPES and ARIPES final states [53].

Figures 3(c) and (d) show the ARPES and ARIPES spectra of WSe_2/Au along the Γ–*M* and Γ–*K* directions. The VBM_Γ, CBM_Γ, VBM_K, and CBM_K of WSe_2/Au are found at 1.20 eV BE, −0.90 eV BE, 1.00 eV BE, and −0.75 eV BE, respectively. Accordingly, the electronic gaps $E_{g,\Gamma}$ and $E_{g,K}$ of WSe_2/Au are 2.10 eV and 1.75 eV, respectively. Unlike the case of MoS_2, the WSe_2/Au VBM_K is shifted by a negligible amount (0.01 eV) due to contact with Au, while CBM_K WSe_2/Au (−0.75 eV BE) is reduced by 0.15 eV as compared to WSe_2/sapphire (−0.90 eV BE). This can be interpreted as the WSe_2/Au appearing more n-type compared to WSe_2/sapphire. In addition, these results show a decrease of $E_{g,K}$ by 0.14 eV on Au. This value is lower as compared to the change of $E_{g,K}$ (0.21 eV) determined for MoS_2 on sapphire versus Au. As the screening of ARPES and ARIPES final states for MoS_2 and WSe_2 by the metal electrons is expected to be the same, the different electronic gap reduction for the two TMDCs must have other origins. While we have no direct evidence for pronounced charge transfer between Au and the two TMDC monolayers, small charge exchange could yet invoke band gap renormalization [52]. In addition, all E_g values of this study decreased notably—depending on the change of dielectric environment - except for $E_{g,\Gamma}$ in MoS_2. This phenomenon likely originates from hybridization between the VBM of MoS_2 and Au at the Γ point. This was shown by Bruix *et al* who reported in a theory study that the interaction with a metallic support strongly distorts the VBM at the Γ point and reduces the $E_{g,K}$ with respect to a free-standing layer, in very good agreement with our experimental results [52].

To obtain $E_{b,exc}$, we also need to know the fundamental exciton transition energy of the TMDCs on the metallic and dielectric supports. At room temperature, the absorptive optical response close to the band edges in TMDCs is known to be strongly dominated by excitons, with only a faint contribution due to trions at slightly lower energies than the main exciton transition [54]. In particular, MoS_2 and WSe_2 exhibit two prominent excitonic features, termed A and B excitons, which stem from transitions at the K-point. The energy difference between A and B is caused by valence band splitting due to spin–orbit coupling [19]. In the following, we focus on the energy range of these A and B resonances and do not consider higher excitations. To obtain the excitonic transition energies, E_{exc}, we performed reflectance measurements as shown in figure 4, which displays measured data (dashed lines) and their first derivative (solid lines) to clearly identify the transition energies, particularly on Au, where the features are less pronounced. In figures 4(a) and (c), MoS_2 and WSe_2 on sapphire show the known excitonic transitions due to the strong light–matter interaction associated with van Hove singularities of their density of states [55]. The respective peak maxima yield 1.87 eV and 2.02 eV for MoS_2, and 1.65 eV and 2.05 eV for WSe_2 of the A and B excitons, respectively. These values of E_{exc} are in agreement with earlier results obtained for these TMDCs on insulators, such as sapphire, fused silica, and quartz [32, 56, 57]. Additionally performed PL measurements showed a peak maximum at the reported literature values corresponding to the exciton transition in these TMDCs (see SI) [58, 59].

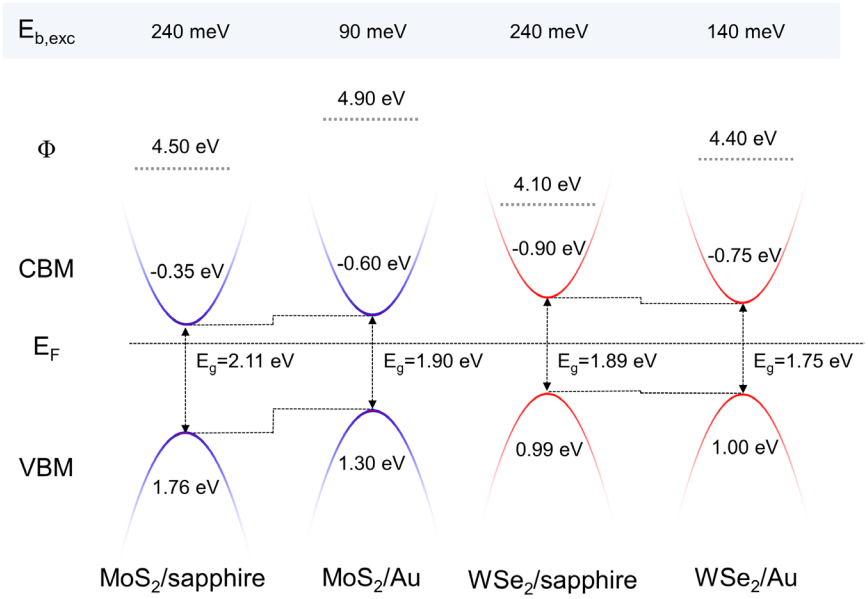

Figure 5. Energy level diagram of MoS_2/sapphire, MoS_2/Au, WSe_2/sapphire, and WSe_2/Au. All values are given at the K-point.

The reflectance spectra of MoS_2 and WSe_2 monolayers on Au show less pronounced excitonic peaks due to the strong background, as evident from figures 4(b) and (d). The proximity of the metal, and possibly a small charge transfer as noted above, substantially influence the optical signature. Yet remarkably, the exciton energies barely change, also in agreement with the result of Mertens *et al* [60]. Accordingly, the transition energies of the A and B excitons, respectively, are determined to be 1.81 eV and 1.95 eV for MoS_2/Au, and 1.61 eV and 1.99 eV for WSe_2/Au.

The most important parameters obtained in this study and the energy level diagrams at the K-point, including the sample work function, are summarized in figure 5 (further details are contained in the SI). On sapphire, the directly determined $E_{b,exc}$ amounts to 240 meV for both MoS_2 and WSe_2, while on Au it is strongly reduced to be 90 meV for MoS_2 and 150 meV for WSe_2, respectively. This observed reduction of $E_{b,exc}$ is in line with previously suggested models [20, 30, 61]. Notably, theoretical calculations of $E_{b,exc}$ for MoS_2 and WSe_2 predicted values of 540 meV–770 meV and 740 meV, respectively [3, 62], which is more than ca. 300 meV higher than determined in the present study. This difference is due to the fact that the calculations did not include any dielectric medium in proximity to the TMDCs, although this is predominantly the case in device structures. In addition, combined experimental and theoretical studies also demonstrated negligible change in exciton binding energy under strain [62, 63] This implies that strong changes in the band structure (and most specifically change of E_g) due to strain should lead to the same changes in E_{exc}. As this is not observed, we can rule out the effect of strain in the observed changes in E_g and in $E_{b,exc}$ reduction as determined in the present study. In other previous studies, optical measurements for MoS_2 and WSe_2 supported on insulator substrates were analyzed using the hydrogenic Rydberg model, which gave indirect estimations of $E_{b,exc}$ with values in the range of 280 meV–440 meV (MoS_2) and 240 meV–370 meV (WSe_2), in fair agreement with our values from a direct determination [32, 64–66]. Unfortunately, $E_{b,exc}$ values derived with this model for these two TMDCs on metal substrates are not available and preclude further comparison.

Regarding the energy levels, MoS_2 on sapphire exhibits apparent n-type character and a high ionization energy (IE) of 6.26 eV, which agrees with the results from Berg *et al* [38]. The IE of MoS_2/Au, WSe_2/sapphire, and WSe_2/Au are found be 6.20 eV, 5.09 eV, and 5.40 eV, respectively. However, the IE values should be used with care, as the TMDCs monolayers did not cover the substrates completely, and the work function (used to determine IE) is an area-average. We suggest considering an error margin of up to 0.5 eV. From the energy level diagrams in figure 5 we can see that substantial energy barriers for the injection of both electrons and holes from Au into MoS_2 and WSe_2 exist, highlighting the need to engineer ways for improved carrier injection from such electrodes. Until now, several 2D TMDCs energy level diagrams derived from photoemission are available, however only from measurements at the Γ point [67–69]. As the actual VBM and CBM minima of the two materials investigated here occur at the K-point, such level diagrams over-estimate injection barriers. Consequently, the diagrams of figure 5 based on ARPES and ARIPES measurements at the K-point are more relevant for understanding the characteristics of TMDCs-based devices.

To summarize, we directly determined $E_{b,exc}$ from E_g and E_{exc} measurements for MoS_2 and WSe_2 monolayers on sapphire and Au substrates. With ARPES and ARIPES measurements, we provide experimental

evidence that the K-point features the minimum and direct band gap. The evaluated E_g and $E_{b,exc}$ values are 2.11 eV and 240 meV for MoS_2/sapphire and 1.89 eV and 240 meV for WSe_2/sapphire, respectively. Owing to improved dielectric screening and possibly a small charge transfer when placing the monolayers on Au, a significant decrease in E_g by 0.21 eV and 0.14 eV was measured for MoS_2 and WSe_2, respectively. Notably, the exciton energy is barely affected by the metal substrate in comparison to the insulating sapphire. Consequently, on Au we observe a huge reduction of $E_{b,exc}$ for MoS_2 and WSe_2 by 150 meV and 100 meV, respectively. As a result, $E_{b,exc}$ determined to be 90 meV for MoS_2 on Au and 140 meV for WSe_2 on Au, respectively. Accordingly, the present results serve as a benchmark in order to evaluate models to derive the exciton binding energies in alternative ways, e.g. the hydrogenic Rydberg model and its extensions, particularly for the case of coupling TMDCs with metallic substrates. In terms of energy levels, MoS_2/Au shows a more p-type character as compared to the apparent n-type one on sapphire. In contrast, WSe_2 appears almost intrinsic on both substrates. The present results help to rationalize the excitonic properties of 2D TMDCs in different dielectric environments and will be useful for designing optoelectronic devices based on this class of intriguing materials.

Acknowledgment

This work was supported by the DFG (SFB951 and AM 419/1-1).

Author contributions

SP wrote the manuscript; collected and analyzed all of the data presented in this manuscript under the supervision of EJLK and NK; NM and SB performed and analyzed the optical experiments. SP and TS performed ARPES, ARIPES experiments and DFT calculations. PA revised the manuscript. AH, AA and LL prepared the TMDC samples for measurement. All authors participated in the discussion and interpretation of the results and commented on the manuscript.

Notes

The authors declare no competing financial interest.

ORCID iDs

Soohyung Park https://orcid.org/0000-0002-6589-7045
Thorsten Schultz https://orcid.org/0000-0002-0344-6302
Patrick Amsalem https://orcid.org/0000-0002-7330-2451
Norbert Koch https://orcid.org/0000-0002-6042-6447

References

[1] Wang Q H, Kalantar-Zadeh K, Kis A, Coleman J N and Strano M S 2012 *Nat. Nanotechnol.* **7** 699–712
[2] Chhowalla M, Shin H S, Eda G, Li L-J, Loh K P and Zhang H 2013 *Nat. Chem.* **5** 263–75
[3] Ramasubramaniam A 2012 *Phys. Rev.* B **86** 115409
[4] Zhang C, Chen Y, Johnson A, Li M-Y, Li L-J, Mende P C, Feenstra R M and Shih C-K 2015 *Nano Lett.* **15** 6494–500
[5] Zhu B, Chen X and Cui X 2015 *Sci. Rep.* **5** 9218
[6] Brus L E 1984 *J. Chem. Phys.* **80** 4403
[7] Wang F 2005 *Science* **308** 838–41
[8] Rigosi A F, Hill H M, Rim K T, Flynn G W and Heinz T F 2016 *Phys. Rev.* B **94** 75440
[9] Palummo M, Bernardi M and Grossman J C 2015 *Nano Lett.* **15** 2794–800
[10] Mak K F, Lee C, Hone J, Shan J and Heinz T F 2010 *Phys. Rev. Lett.* **105** 2–5
[11] Evans B L and Young P A 1965 *Proc. R. Soc.* A **284** 402–22
[12] Splendiani A, Sun L, Zhang Y, Li T, Kim J, Chim C Y, Galli G and Wang F 2010 *Nano Lett.* **10** 1271–5
[13] Lin Y, Ling X, Yu L, Huang S, Hsu A L, Lee Y-H, Kong J, Dresselhaus M S and Palacios T 2014 *Nano Lett.* **14** 5569–76
[14] Mak K F, He K, Lee C, Lee G H, Hone J, Heinz T F and Shan J 2013 *Nat. Mater.* **12** 207–11
[15] Ross J S *et al* 2013 *Nat. Commun.* **4** 1474
[16] You Y, Zhang X-X, Berkelbach T C, Hybertsen M S, Reichman D R and Heinz T F 2015 *Nat. Phys.* **11** 477–81
[17] Bernardi M, Palummo M and Grossman J C 2013 *Nano Lett.* **13** 3664–70
[18] Zhao W, Ghorannevis Z, Chu L, Toh M, Kloc C, Tan P-H and Eda G 2013 *ACS Nano* **7** 791–7
[19] Tongay S, Zhou J, Ataca C, Liu J, Kang J S, Matthews T S, You L, Li J, Grossman J C and Wu J 2013 *Nano Lett.* **13** 2831–6
[20] Kylänpää I and Komsa H-P 2015 *Phys. Rev.* B **92** 205418
[21] Ross J S *et al* 2014 *Nat. Nanotechnol.* **9** 268–72
[22] Hang H and Koch S W 2009 *Quantum Theory of the Optical and Electronic Properties of Semiconductors* 5th edn (Singapore : World Scientific)
[23] Dvorak M, Wei S-H and Wu Z 2013 *Phys. Rev. Lett.* **110** 16402
[24] Shan W, Little B, Fischer A, Song J, Goldenberg B, Perry W, Bremser M and Davis R 1996 *Phys. Rev.* B **54** 16369–72
[25] Yu P Y and Cardona M 2010 *Fundamentals of Semiconductors* (*Graduate Texts in Physics*) 4th edn (New York: Springer)
[26] Ye Z, Cao T, O'Brien K, Zhu H, Yin X, Wang Y, Louie S G and Zhang X 2014 *Nature* **513** 214–8
[27] Cheiwchanchamnangij T and Lambrecht W R L 2012 *Phys. Rev.* B **85** 205302
[28] Ugeda M M *et al* 2014 *Nat. Mater.* **13** 1091–5
[29] Zhang C, Johnson A, Hsu C L, Li L J and Shih C K 2014 *Nano Lett.* **14** 2443–7
[30] Raja A *et al* 2017 *Nat. Commun.* **8** 15251
[31] Chernikov A, Berkelbach T C, Hill H M, Rigosi A, Li Y, Aslan O B, Reichman D R, Hybertsen M S and Heinz T F 2014 *Phys. Rev. Lett.* **113** 76802
[32] Liu H-L, Shen C-C, Su S-H, Hsu C-L, Li M-Y and Li L-J 2014 *Appl. Phys. Lett.* **105** 20190
[33] Perebeinos V, Tersoff J and Avouris P 2004 *Phys. Rev. Lett.* **92** 257402
[34] Berkelbach T C, Hybertsen M S and Reichman D R 2013 *Phys. Rev.* B **88** 45318
[35] Coy-Diaz H, Bertran F, Chen C, Avila J, Rault J, Le Fèvre P, Asensio M C and Batzill M 2015 *Phys. Status Solidi* **9** 701–6
[36] Jin W *et al* 2015 *Phys. Rev.* B **91** 121409
[37] Ramasubramaniam A, Naveh D and Towe E 2014 *Phys. Rev.* B **84** 205325
[38] Shi L-B, Li M-B, Xiu X-M, Liu X-Y, Zhang K-C, Liu Y-H, Li C-R and Dong H-K 2017 *J. Appl. Phys.* **121** 205305
[39] Chernikov A, van der Zande A M, Hill H M, Rigosi A F, Velauthapillai A, Hone J and Heinz T F 2015 *Phys. Rev. Lett.* **115** 126802
[40] Eknapakul T *et al* 2014 *Nano Lett.* **14** 1312–6
[41] Wang C Q, Chen W G, Zhang Y S, Sun Q and Jia Y 2015 *Tribol. Lett.* **59** 8

[42] Klein J, Wierzbowski J, Regler A, Becker J, Heimbach F, Müller K, Kaniber M and Finley J J 2016 *Nano Lett.* **16** 1554–9
[43] Radisavljevic B and Kis A 2013 *Nat. Mater.* **12** 815–20
[44] Vella D *et al* 2017 *2D Mater.* **4** 21005
[45] Zhou S Y, Gweon G-H, Spataru C D, Graf J, Lee D-H, Louie S G and Lanzara A 2005 *Phys. Rev.* B **71** 161403
[46] Zhang Y *et al* 2016 *Nano Lett.* **16** 2485–91
[47] Jin W *et al* 2013 *Phys. Rev. Lett.* **111** 106801
[48] Singh A K, Hennig R G, Davydov A V and Tavazza F 2015 *Appl. Phys. Lett.* **107** 53106
[49] Zhou W, Zou X, Najmaei S, Liu Z, Shi Y, Kong J, Lou J, Ajayan P M, Yakobson B I and Idrobo J C 2013 *Nano Lett.* **13** 2615–22
[50] Dolui K, Rungger I and Sanvito S 2013 *Phys. Rev.* B **87** 1–7
[51] Song Z *et al* 2017 *ACS Nano* **11** 9128–35
[52] Bruix A *et al* 2016 *Phys. Rev.* B **93** 165422
[53] Bhanu U, Islam M R, Tetard L and Khondaker S I 2015 *Sci. Rep.* **4** 5575
[54] Zhang C, Wang H, Chan W, Manolatou C and Rana F 2014 *Phys. Rev.* B **89** 205436
[55] Britnell L *et al* 2013 *Science* **340** 1311–4
[56] Li Y, Chernikov A, Zhang X, Rigosi A, Hill H M, Van Der Zande A M, Chenet D A, Shih E M, Hone J and Heinz T F 2014 *Phys. Rev.* B **90** 205422
[57] Kozawa D *et al* 2014 *Nat. Commun.* **5** 4543
[58] Zhang Q *et al* 2017 *ACS Nano* **11** 10808–15
[59] Yan T, Qiao X, Liu X, Tan P and Zhang X 2014 *Appl. Phys. Lett.* **105** 101901
[60] Mertens J, Shi Y, Molina-Snchez A, Wirtz L, Yang H Y and Baumberg J J 2014 *Appl. Phys. Lett.* **104** 191105
[61] Olsen T, Latini S, Rasmussen F and Thygesen K S 2016 *Phys. Rev. Lett.* **116** 56401
[62] Shi H, Pan H, Zhang Y-W and Yakobson B I 2013 *Phys. Rev.* B **87** 155304
[63] Conley H J, Wang B, Ziegler J I, Haglund R F, Pantelides S T and Bolotin K I 2013 *Nano Lett.* **13** 3626–30
[64] Yu Y *et al* 2015 *Sci. Rep.* **5** 16996
[65] Hill H M, Rigosi A F, Roquelet C, Chernikov A, Berkelbach T C, Reichman D R, Hybertsen M S, Brus L E and Heinz T F 2015 *Nano Lett.* **15** 2992–7
[66] He K, Kumar N, Zhao L, Wang Z, Mak K F, Zhao H and Shan J 2014 *Phys. Rev. Lett.* **113** 26803
[67] Tao J, Chai J W, Zhang Z, Pan J S and Wang S J 2014 *Appl. Phys. Lett.* **104** 232110
[68] Chen C-H, Wu C-L, Pu J, Chiu M-H, Kumar P, Takenobu T and Li L-J 2014 *2D Mater.* **1** 34001
[69] Arramel , Yin X, Wang Q, Zheng Y J, Song Z, bin Hassan M H, Qi D, Wu J, Rusydi A and Wee A T S 2017 *ACS Appl. Mater. Interfaces* **9** 5566–7